Mitigating valley-driven localization in atomically thin dopant chains in Si

Amintor Dusko,* A. L. Saraiva, and Belita Koiller
Instituto de Física, Universidade Federal do Rio de Janeiro, Caixa Postal 68528, 21941-972 Rio de Janeiro, Brazil
(Received 31 March 2016; revised manuscript received 8 August 2016; published 19 September 2016)

A theoretical study of the localization properties of nanowires of dopants in silicon (Si) fabricated by ionic implantation or scanning tunnel microscope lithography is presented for a model incorporating the currently unavoidable imprecision in individual donor positioning. Experiments have shown that Ohm's law holds in some cases, in apparent defiance to the Anderson localization theory in one dimension. We investigate how valley interference affects the traditional theory of electronic structure of disordered systems. Each isolated donor orbital is realistically described by multivalley effective-mass theory. We extend this model to describe chains of donors as a linear combination of dopant orbitals. Disorder in donor positioning is taken into account, leading to an intricate disorder distribution of hoppings between nearest-neighbor donor sites (donor-donor tunnel coupling)—an effect of valley interference. A decay length, related to the usual localization length, is obtained for phosphorous (P) donor chains from a transfer-matrix approach and is further compared with the chain length. We quantitatively determine the impact of uncertainties δR in the implantation position relative to a target and also compare our results with those obtained without valley interference. We analyze systematically the aimed interdonor separation dependence (R_0) and show that fairly diluted donor chains ($R_0 = 7.7$ nm) may be as long as 100 nm before the effective onset of Anderson localization, as long as the positioning error is under a lattice parameter ($\delta R < 0.543$ nm).

DOI: 10.1103/PhysRevB.94.115425

I. INTRODUCTION

On demand fabrication of dopant arrangements in silicon is made possible by recent scanning tunnel microscope (STM) lithography techniques. Nanowires constructed with this technique obey Ohm's law, in apparent defiance to the Anderson localization theorem [1,2]. Even in quasi-one-dimensional systems constructed through ionic implantation of donors, for which positional disorder is significantly larger, metal-insulator transition is observed at large enough dopant densities [3–5]. It is unclear what aspects of the host semiconductor drives this behavior and what we can do to effectively engineer these transport properties.

We consider here a system of dopants deliberately implanted aiming at target positions so as to regulate interdonor tunnel coupling (or hopping). Our model incorporates the currently unavoidable imprecisions in donor positions and, in particular, how they manifest in the hopping distribution. We develop a theory of linear combinations of dopant orbitals (LCDO), in which each donor orbital is described within multivalley effective-mass theory (MV-EMT) including a central cell correction. We then obtain the transfer matrix for donor chains with realistic positioning disorder models and extract the decay length for finite chains based on the behavior of the Lyapunov exponent of the transformation defined by it. We compare systems with and without valley interference, showing that valleys play two opposite roles in the localization of states—it increases the number of states available at the point of charge neutrality (half-filled band) and introduces the possibility of fully destructive interference, leading to a broken link in the chain and reducing the paths through which the current can percolate. We also study effects of uncertainty in positioning in two and three dimensions (a disk or a sphere of uncertainty), consistent with bottom-up STM lithography and top-down ionic donor implantation methods, respectively.

II. DONORS IN SILICON WITHIN EFFECTIVE MASS

We construct here the model for the electronic structure of dopant chains extending the EMT of donor impurities in Si. First, we revise the central cell corrected model of an impurity in silicon within effective mass (Sec. II A). We also revise how to construct the wave function of a donor pair from a single dopant orbital, in analogy with the molecular orbital theory. Then this analogy is extended into the model of a chain of atoms, with a wave function described as a linear combination of central cell corrected Kohn-Luttinger wave functions centered at the impurity sites, which we dub LCDO.

A. Single donor

A distinct feature of the Si band structure is the sixfold degeneracy of the conduction-band edge, located at $\mathbf{k}_\mu$ along the $\langle 100\rangle$ directions, $\mu = \pm x, \pm y, \pm z$ with $|\mathbf{k}_\mu| = k_0 = 0.85(\frac{2\pi}{a_{\rm Si}})$ in the fcc Brillouin zone ($a_{\rm Si} = 0.5431$ nm is the conventional fcc lattice parameter for Si). [6] For bulk Si, the periodic Hamiltonian does not couple the valleys, which remain degenerate. A substitutional donor breaks the translational symmetry and the steep donor potential couples different valleys, resulting in a nondegenerate ground state to which the six valleys contribute equally (A_1 symmetry). The $A1$ state is well separated (12 meV) from the first excited state.

Kohn and Luttinger [7] (KL) proposed, within effective-mass theory (EMT), a ground-state variational wave function pinned at the donor position with the correct A_1-symmetry written in terms of hydrogenic envelopes and Bloch functions for each conduction-band minimum. For a donor at $\mathbf{r} = 0$,

$$\Psi_{\rm KL}(\mathbf{r}) = \frac{1}{\sqrt{6}} \sum_{\mu=1}^{6} F_\mu(\mathbf{r}) e^{i\mathbf{k}_\mu\cdot\mathbf{r}} u_\mu(\mathbf{r}), \qquad (1)$$

*amintor.dusko@gmail.com

where $F_\mu(\mathbf{r})$ are hydrogeniclike envelope functions and $u_\mu(\mathbf{r})$ are the periodic parts of the six Bloch functions. The effective-mass anisotropy affects the ground-state envelope functions, suggesting the use of deformed $1s$ orbitals with a and b as variational parameters,

$$F_{\pm z}(\mathbf{r}) = \frac{1}{\sqrt{\pi a^2 b}} \exp\left(-\sqrt{\frac{x^2+y^2}{a^2}+\frac{z^2}{b^2}}\right), \qquad (2)$$

and equivalently to $F_{\pm x}$ and $F_{\pm y}$. A similar variational envelope was proposed by Kittel and Mitchell [8].

This gives a species-independent description and a sixfold degenerate donor ground state—in contrast, experiments show a variation in binding energies among different group-V dopants (P, As, Sb, Bi) and a nondegenerate ground state as mentioned before. Both problems are corrected by a species-dependent central cell potential, which accounts for the more attractive potential close to the donor site, where the screening by the core electrons is less effective. Besides splitting the $1S$ manifold into a nondegenerate $A1$ state and three- and twofold degenerate excited states ($T2$ and E, respectively) at the experimentally observed energies, the main consequence of this correction to the present study is to contract the donor ground-state wave function—an effect confirmed experimentally [9]. The central cell prescription discussed in Ref. [10] is incorporated in our model calculations below.

B. Donor pairs and linear arrays

In analogy with the standard linear combination of atomic orbitals (LCAO) scheme in quantum chemistry, we construct the wave function of a pair of donors as a linear combination of dopant orbitals (LCDO) described in Eq. (3) centered at the substitutional donor sites $\mathbf{r_1}$ and $\mathbf{r_2}$. The dopant pair (molecule) variational wave function reads

$$\Psi_{\rm mol}(\mathbf{r}) = \alpha_1 \Psi_{\rm KL}(\mathbf{r}-\mathbf{r_1}) + \alpha_2 \Psi_{\rm KL}(\mathbf{r}-\mathbf{r_2}) \qquad (3)$$

and the coefficients α_1 and α_2 must be determined variationally, under the normalization constraint $\langle\Psi_{\rm mol}|\Psi_{\rm mol}\rangle = 1$. As in the LCAO procedure, this leads to a set of Rothaan equations for the coefficients [11], which can be written as a Fock matrix $\mathbf{F}$ and an overlap matrix $\mathbf{S}$. Here we are interested in the single-particle effects, so that the Fock operator is the single electron Hamiltonian.

This approach is valid as long as (i) the interdonor distance $\mathbf{R_{12}} = \mathbf{r_2} - \mathbf{r_1}$ is not too small, so that the assumptions of EMT are still valid (continuum approximation); and (ii) the ground-state wave function is still mainly composed of a symmetric combination of valley states pinned around each site. The latter assumption is more restrictive—while the actual ground-state combination of valleys slowly changes as the donors are brought closer together [12], near a distance $R_{12} \approx 6$ nm there is a sudden change from a mostly A_1-like to mostly T_2-like combination of valleys [12]. Therefore, our model is qualitatively inaccurate below this interdonor distance.

If we call $|1\rangle$ and $|2\rangle$ the orbitals centered in each donor, the pair Hamiltonian within a one-electron LCDO description may be written as

$$\widehat{H}_{\rm pair} = \epsilon\,[|1\rangle\langle 1| + |2\rangle\langle 2|] + t\,[|1\rangle\langle 2| + |2\rangle\langle 1|], \qquad (4)$$

where ϵ is the isolated donor eigenenergy, which may be taken as the energy origin, and t is the tunneling or hopping energy, which is a function of the donors relative position $\mathbf{R}_{12}$. These LCDO parameters are explicitly obtained semiempirically, as discussed below. This procedure may be extended for larger sets of dopants.

We formulate a simple one-orbital per site LCDO Hamiltonian for linear arrays of well separated donors based on nearest-neighbor pair considerations. To describe the array's ground-state properties it remains acceptable to restrict the basis set to the ground-state orbital in each donor, since the perturbation due to nearby donors is relatively small. Further approximations aiming at simplifying the numerical LCDO parameters calculations are discussed in Sec. III.

Following (4), we write a nearest-neighbors LCDO Hamiltonian in the basis set of the $A1$ KL variational solutions, as given in Eq. (1), to describe the ground state of a linear array of hydrogeniclike impurities,

$$\widehat{H} = \sum_{\langle i,j\rangle}\left[\frac{1}{2}\epsilon\, n_i + t_{i,j}(c_i^\dagger c_j + c_j^\dagger c_i)\right], \qquad (5)$$

where ϵ is the on-site energy (site-independent for a single donor species) and $t_{i,j}$ is the nearest-neighbor hopping, t in Eq. (4), for donors at sites i and j. We allow the tunnel coupling to be dependent on the particular pair, incorporating possible displacements of donors' relative positions along the fabrication procedure, so that $t_{i,j} = t(\mathbf{R}_{ij})$. The creation ($c_i^\dagger$) and annihilation ($c_i$) operators refer to the occupation of the orbital $|i\rangle$ at site i, thus $n_i = c_i^\dagger c_i$ is the site occupation operator.

III. CALCULATION OF LCDO PARAMETERS—SINGLE vs MULTIVALLEY MODEL

It is possible to obtain, within plausible approximations, analytic expressions for the LCDO parameters. The first approximation is to assume isotropic envelopes by taking $a = b = a_{cc}$, where the subscript cc refers to the effective Bohr radius obtained from a central cell corrected potential [10], given in Table I. We do this for each of the valleys separately, preserving the conduction-band sixfold degeneracy and the physical insight on valley degeneracy effects, e.g., valley interference. Furthermore, we focus here on dilute doping, which is easily accessible within effective mass (as opposed to the dense limit [2]). Within this dilute limit, the

TABLE I. Single donor ground-state binding energy (E_0) and effective Bohr radius (see text) for group-V dopants as given and described in Ref. [10].

Donor	E_0 (meV)	a_{cc} (nm)
P	45.58	1.106
As	53.77	0.815
Sb	42.71	1.241
Bi	70.88	0.580

orbital overlap is small enough to be treated perturbatively. Therefore we dismiss hoppings among donors that are not nearest neighbors.

To calculate the matrix elements of the atomistic Hamiltonian for a one-dimensional array of N donors $\langle j|\hat{H}|i\rangle$, we rewrite $\hat{H} = \hat{H}_i + \hat{H}'$, where $\hat{H}' = \sum_{j\neq i} \hat{V}_j$ is the perturbation potential due to all other cores and $\hat{H}_i = \hat{K} + \hat{V}_i$ consists of the kinetic energy ($\hat{K}$) plus the core potential $\hat{V}_i$ for donor i. This is useful because, by construction, $\hat{H}_i|i\rangle = -E_0\,|i\rangle$ where E_0 is the single donor binding energy.

Since $\langle j|\hat{H}'|i\rangle \ll \langle j|\hat{H}_i|i\rangle$, the perturbation term is neglected in the hopping energy expression, resulting in

$$t_{ij} = \langle j|\hat{H}_i|i\rangle + \langle j|\hat{H}'|i\rangle, \tag{6a}$$

$$\approx -E_0\, S(R_{ij}, a_{cc}). \tag{6b}$$

So t_{ij} is a function of the single donor ground-state binding energy (E_0) and the overlap between $|i\rangle$ and $|j\rangle$ nearest-neighbors orbitals $S(R_{ij}, a_{cc}) = \langle i\,|\,j\rangle$.

If energies are measured from the bottom of the conduction band, we would identify ϵ with $-E_0$. Instead, we set the origin of energies to the center of the impurity band setting $\epsilon = 0$, without loss of generality.

In order to highlight valley interference effects in our one-electron–one-orbital isotropic envelopes model, we consider two expressions for the hopping (we omit the i, j labels when no ambiguity is raised). First we take an expression neglecting valley interference effects, equivalent to the dopant orbitals appearing on single valley semiconductors [10],

$$t^{sv} = E_0\, e^{-R/a_{cc}} \left(1 + \frac{R}{a_{cc}} + \frac{R^2}{3a_{cc}^2}\right). \tag{7}$$

In this case t is a function of $|\mathbf{R}| = R$ only. The expression for the overlap is simply that of an H_2 molecule with orbital radius and energies rescaled by the material effective parameters.

The second approach considers the sixfold degenerate Si valleys giving, for isotropic envelopes,

$$t^{mv} = t^{sv} \left[\frac{1}{3}\sum_{\eta=1}^{3} \cos(k_0\, R_\eta)\right], \tag{8}$$

referred to as the multivalley (mv) model. Here R_η ($\eta = x, y, z$) are the Cartesian coordinates of $\mathbf{R}$ along the Si cubic axes. Interference among the six Bloch functions manifests itself as the term in square brackets, resulting in an oscillatory behavior of the tunnel coupling. Depending on the vector $\mathbf{R}$, strong suppression of the tunnel coupling may occur. Figure 1 presents the hopping energy connecting a pair of donors a distance R_0 apart along three crystal directions ([100], [110], and [111]). Note that the more localized Bi donor orbitals leads to a negligible coupling as compared to the other donor species.

For each eigenstate $\Psi(x)$, we define a decay length (ξ) from the asymptotic behavior of the wave function, presumed to be of the form

$$\Psi(x) \to \exp\,[-|x|/\xi]. \tag{9}$$

This form of decay applies to exactly infinite chains, in which ξ plays the role of the usual localization length. It describes the spatial extent of the wave function, and is thus closely linked with transport properties.

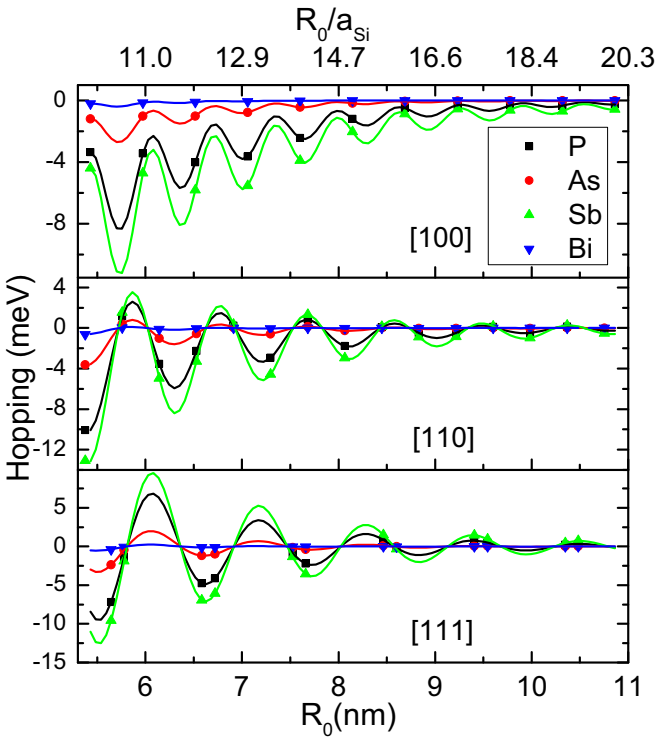

FIG. 1. Hopping (t^{mv}) as a function of the distance between group-V (P, As, Sb, and Bi) donor pairs along the given crystal directions. Symbols represent the available positions in the Si lattice for substitutional donors.

Experiments are performed in real finite chains. We formally determine a decay length in finite chains by the standard transfer-matrix approach. Our criterion for transport in finite chains, stated in Sec. VI, compares ξ to the chain length L.

IV. TRANSFER-MATRIX APPROACH

The transfer-matrix approach (TMA) is an efficient way to calculate the localization lengths in one-dimensional (1D) chains and is easily extended to quasi-1D structures [13–18]. A very concise description of the operational steps involved is given here.

We write the eigenfunctions in the basis of $A1$ orbitals as $|\Psi\rangle = \sum_n \phi_n|n\rangle$, where n is the index for the chain site. The TMA approach [14,19,20] follows from the relation among the wave-function amplitudes ϕ_n, $t_{n,n-1}\phi_{n-1} + t_{n,n+1}\phi_{n+1} = E\phi_n$, which is directly cast into a tensorial formulation,

$$\widehat{\Phi}_n = \begin{pmatrix} \phi_{n+1} \\ \phi_n \end{pmatrix}, \qquad \widehat{\Phi}_n = \widehat{T}_n \cdot \widehat{\Phi}_{n-1}, \tag{10a}$$

$$\widehat{T}_n = \begin{pmatrix} E/t_{n,n+1} & -t_{n,n-1}/t_{n,n+1} \\ 1 & 0 \end{pmatrix}, \tag{10b}$$

$$\widehat{\Phi}_{L-1} = \left(\prod_{i=1}^{L} \widehat{T}_{L-i}\right) \cdot \widehat{\Phi}_0. \tag{10c}$$

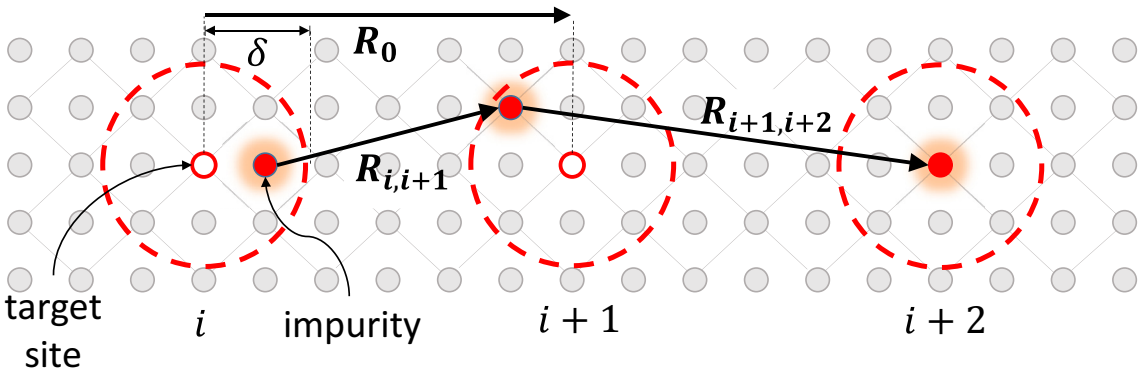

FIG. 2. Schematic representation of our model of disorder: target sites (small open circles in red solid lines) are aligned along a single [110] axis and separated by $\mathbf{R_0}$. Dashed circles of radius δ centered at each target site define the uncertainty region. In two dimensions the actual donor position is randomly picked among the substitutional sites inside this disk (grey circles and target). In the 3D disorder model the position is picked inside a sphere of radius δ. Relative position vectors for consecutive sites are indicated.

These relations show that indeed $\widehat{T}$ acts as a transfer operator for the Lyapunov vectors ($\widehat{\Phi}_n$), while (10c) is guaranteed to asymptotically converge by the Oseledec theorem [21–24].

The mapping described in Eq. (10c) defines how the wave function decays from a reference site $i = 0$ into $i = L$. Therefore, we can relate the localization length ξ and the Lyapunov characteristic exponents (LCEs) γ_p, with $p = 0,1$, for both components of the vector. The LCEs are calculated numerically, as discussed in Appendix.

Once the mapping has converged, any iteration like (10a) gives $\widehat{\Phi}_n^{(p)} = \exp[\gamma_p \cdot |\mathbf{R}_n|] \cdot \widehat{\Phi}_{n-1}^{(p)}$, where the index p refers to each LCE and $|\mathbf{R}_n|$ is the distance between consecutive sites $(n-1,n)$. The LCEs lead to solutions interpreted as either an increasing wave function (which we call γ_1) or decreasing (γ_0). The unphysical exponent γ_1 is discarded, and the decreasing solution leads to a localization length $\xi = |\gamma_0^{-1}|$.

V. DONOR ARRANGEMENT AND DISORDER

We simulate a (quasi)linear array of substitutional donors in Si along a [110] symmetry direction as sketched in Fig. 2. Target positions are assigned at evenly spaced substitutional atomic sites in the Si structure, with nearest neighbors separated by a vector $\mathbf{R_0}$. In the absence of disorder, the electronic structure is trivially calculated, since in Eq. (5) $t_{i,j} = t(\mathbf{R_0})$, constant for all nearest-neighbors pairs.

In real samples, unavoidable deviations from the target positions lead to a disordered Hamiltonian. Here the most affected terms are the off-diagonal matrix elements, $t_{i,j} = t(\mathbf{R_{ij}})$, which specify our model of disorder, as the hopping distribution is implicitly defined by the donors positions. Positioning disorder is simulated here by a geometric parameter δ (see Fig. 2). Around each target position $n\mathbf{R_0}$, with n integer, a region of uncertainty is taken as a disk or a sphere (we discuss both) of radius δ. The donor is randomly positioned at a substitutional site within the uncertainty region.[1] This approach has the same ingredients found in fabrication methods based on impurity implantation [1,3,4] followed by an annealing procedure (guaranteeing the occupation of the energetically favorable substitutional site).

The amount of disorder is dictated by the accuracy of the donor positioning method. Ionic implantation is characterized by a straggle region in the longitudinal direction and some lateral uncertainty due to imperfect collimation of the accelerated ionic beam [3,4]—which typically leads to a three-dimensional uncertainty region. If instead the nanostructure is fabricated by bottom-up lithographic implantation [1], the uncertainty region is reduced by the far better precision of the lithographic instrument tip. Furthermore, the uncertainty is initially confined to the exposed surface—which we model as a two-dimensional uncertainty disk (in fact, often the overgrowth of Si on top of the donor arrangement and thermal treatment lead to some three-dimensional uncertainty due to diffusion). In both cases, the radius δ establishes the disorder distribution in the electronic Hamiltonian. A more general model would allow an ellipsoidal region, but an estimate of the aspect ratio for each experiment would be needed. Instead, we restrict the study to the special cases of a sphere and a disk in order to obtain general features due to the dimensionality of the diffusion, instead of modeling the peculiarities of each method. Only discrete values of δ, representing a change in the number of lattice sites contained within the sphere/disk, are meaningful. For example, all $\delta < a_{\mathrm{Si}}\sqrt{3}/4$ are equivalent to $\delta = 0$, since all of them only contain the central target site.

Target chains along the [110] direction imply $(R_0)_x = (R_0)_y = n\, a_{\mathrm{Si}}/2$, as in Ref. [1]. The role of donors' density ($\rho = 1/R_0$) is assessed by considering target chains with different linear densities, i.e., changing R_0.

VI. MOBILITY EDGES

Electronic transport in a chain of donors differs from a regular condensed-matter system in many ways. A relevant

[1] A Gaussian distribution with width σ was also attempted, giving essentially the same results for hopping distributions as the uniform case within circle or sphere of radius δ, as long as $\sigma \approx \delta$. It is unclear, though, what is the most realistic distribution model. We therefore adopt the simplest (single parameter), uniform distribution.

aspect is the finiteness of these chains, which may have a length comparable to or lesser than the extent of an exponentially localized state. In the former case, such electronic state would contribute to charge currents and, in the absence of scattering processes, it conducts in the so-called ballistic transport regime. In the presence of relaxation phenomena such as electron-phonon scattering, transport would fit into the Drude or Ohmic transport picture. Our criterion for metallic conductivity is based on these considerations, and we do not explicitly include relaxation.

The mature theory of electronic localization by disorder is discussed extensively in the literature. For infinite 3D disordered systems the theoretical prediction is that, while extended and localized states coexist in the solid, they are completely segregated in energy. Eigenenergies of localized (toward the band edges) and of delocalized (around the band center) states are sharply separated at the so-called mobility edges (μ) [25,26].

In one dimension, disorder of any strength localizes all states. Considering that metallicklike current involves transport by delocalized electrons, it should not be observed in disordered chains, where no mobility edge is present. However, when dealing with *finite* arrays, we may define an effective mobility edge, $\mu_{\rm eff}(L)$, as the value of the energy at which the localization length of the states becomes larger than the chain length L, a scenario compatible with current flow along a disordered 1D system.

In one dimension, our nearest-neighbors model with off-diagonal disorder gives a symmetric distribution of eigenstates with respect to the on-site energy, chosen here as $\epsilon = 0$, so that for $\xi < L$ in all energy domain we get $\mu_{\rm eff} = 0$.

It is also convenient from the theoretical point of view to define the converse quantity. Given an interdonor target spacing R_0 and disorder length δ, we call length edge the limiting length Λ of chains above which any chain show nonconducting behavior, i.e., $\xi(R_0,\delta,L > \Lambda) < L$ for any disorder realization. This requirement for conductivity is sensitive to the particular realization of disorder, as it also happens in experiments, which are in fact quite sample dependent. As a general probe to quantitatively characterize the transport behavior for chains of different lengths (L), target positions (R_0), and degrees of disorder (δ), we calculate Lyapunov exponents for each chain realization in ensembles ($\sim$10 000 chains) for each set L,R_0,δ. With the Lyapunov exponents we obtain an estimate of the decay length (which formally is only well defined in the asymptotic limit of very long chains) and each chain in the ensemble is identified as conducting or not (based on the presence or absence of states deemed conducting). Results in Figs. 3 and 4 give Λ, the length above which all chains in the ensemble are not conducting, not localization lengths or decay lengths directly. The particular proportion of conducting to nonconduction states in each ensemble is explored in Fig. 6, where the percentage of conducting states is given.

Figure 3 shows the length edge dependence on the interdonor separation (Λ vs R_0) for a fixed disorder $\delta = 0.4$ nm. It is possible to observe a nonmonotonic fluctuation behavior, with more pronounced and steeper oscillations for 2D than for 3D disorder. We analyze each of these features next. It is clear that the results here regarding electronic properties

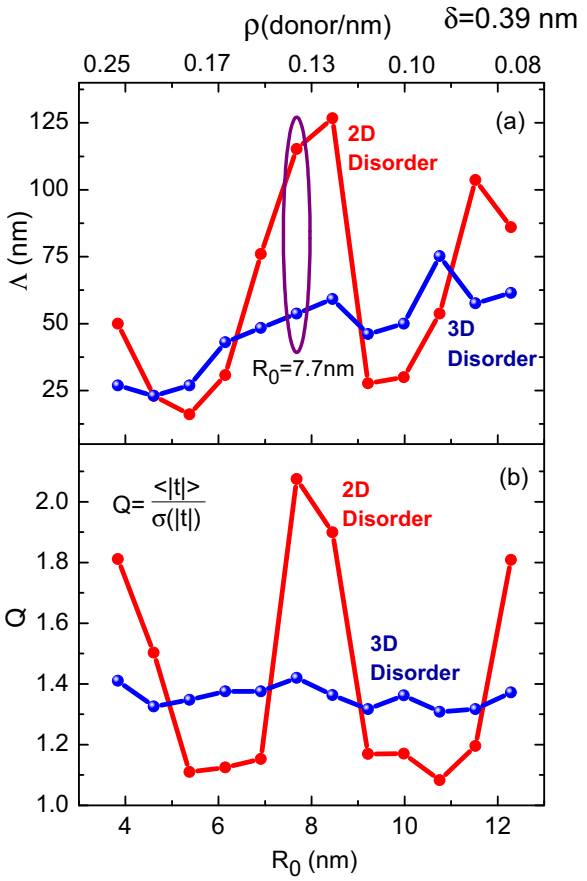

FIG. 3. (a) Length edge (Λ)—the upper limit of length for a chain to sustain electronic transport—as a function of distance between consecutive target positions (R_0) in 2D and 3D disorder models for multivalley hopping and $\delta = 0.4$ nm. The encircled region is explored in Fig. 4 which shows the dependence of Λ on disorder δ for $R_0 = 7.7$ nm. The region below each line is compatible with current-carrying behavior. Error bars are smaller than the data points. (b) Parameter Q vs R_0 follows qualitatively the behavior of Λ above.

are a consequence of the underlying hopping distributions, unambiguously fixed by the chain geometry.

The difference in fluctuations amplitude from 2D to 3D may be understood from of the impact of the dimensionality in the number of different nearest-neighbors relative vector bonds of the chain. In the 2D disorder model, the circle of radius $\delta = 0.4$ nm contains five possible sites for a substitutional impurity in Si—thus 25 relative positions for consecutive donors—among which only nine are inequivalent (lead to different tunnel couplings). In the 3D case, a sphere of radius $\delta = 0.4$ nm contains 17 sites, leading to 289 different relative positions of consecutive pairs, distributed in 36 inequivalent distances, thus 36 possible values for the tunnel coupling. More generally, for a fixed disorder radius δ, there are more possibilities for different vectors $\mathbf{R}_{ij}$ in three dimensions than in two dimensions and, as a result, fluctuations in Λ tend to average out becoming less pronounced in the 3D case, as illustrated in Fig. 3. Reduced fluctuations in three dimensions with respect to otherwise equivalent models in two dimensions are also observed in Figs. 4 and 5, as discussed next.

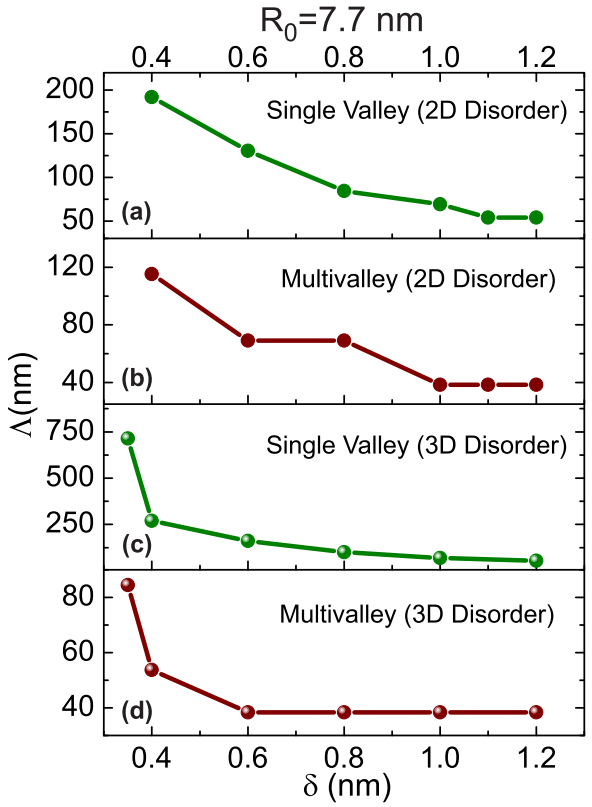

FIG. 4. Disordered chain length edge (Λ) as a function of 2D (3D) disorder radius (δ) for single valley model [(a) and (c)] and multivalley model [(b) and (d)]. Results are presented for a distance $R_0 = 7.7$ nm between consecutive target implantation points.

We now discuss the counterintuitive nonmonotonic fluctuations of Λ vs R_0. We recall that results in Fig. 1 show that, in our nearest-neighbor MV hopping model (both 2D and 3D), the hopping oscillates as it decays exponentially with R_0. Thus larger values of R_0 tend to correspond to (i) a narrower range of hopping elements in absolute value, so a lower degree of disorder which favors transport, but (ii) reduced absolute values of the hopping energies, which decrease exponentially with interdonor distance, inhibiting transport. These competing effects may be roughly connected to (i) the spread [standard deviation (σ)] and (ii) the average of the hopping distribution (with hopping taken in absolute value). As a test of these concepts, we naively assume that the transport capability of a chain varies linearly with the average value of the hopping (in absolute value) and with the inverse of the spread, so the ratio $Q = \langle|t|\rangle/\sigma(|t|)$ would give a figure of merit related to the transport quality in a particular chain. We calculate average and width of the hopping distributions resulting from all possible pairs at each R_0 and δ. The ratio Q is plotted in Fig. 3(b). As can be seen, Q follows reasonably the patterns in Λ on frame (a). Of course we get some local inversions, since there is no justification to state that Q is linear in both $\langle|t|\rangle$ and $1/\sigma(|t|)$, and to ignore other aspects as the value of R_0, since for a fixed length L, larger R_0 chains will contain fewer atoms and bonds, reducing the number of tunnel steps, favoring transport.

The effect of increasing disorder on the maximum chain length Λ is investigated in Fig. 4 for fairly dilute donor chains ($R_0 = 7.7$ nm). Here we note a decrease in Λ with increasing disorder, a plausible result. Again, the 2D data points show distinct fluctuations as compared to the smoother 3D cases. We discuss general trends in Λ in Sec. VII.

VII. GENERAL TRENDS FOR 2D AND 3D MODELS

Figure 3 also highlights that the 2D disorder model leads to longer conducting chains, compared to 3D disorder. But the difference between these models is not too large, revealing that a 3D diffusion is not significantly more damaging to transport than the 2D one.

In Fig. 4 different valley compositions and dimensionalities are compared in terms of how they affect Λ. In the multivalley model at fixed $R_0 = 7.7$ nm, the trend $\Lambda_{2D} > \Lambda_{3D}$ is preserved for all considered disorder parameters $\delta > 0.4$ nm, as illustrated in Figs. 4(b) and 4(d). In order to appreciate valley interference effects, results within the single valley model are also presented in Fig. 4, showing that the general decay of Λ with disorder is similar to the multivalley description. Note that, for each δ, single valley models lead to larger values of Λ as compared to multivalley ones, consistent with destructive valley interference affecting the hopping. We remark that, for this particular R_0, the 3D disorder model sustains larger Λ values [see Figs. 4(a) and 4(c)]. It is possible that this ordering inverts at some value of R_0 as in the multivalley case, a question that is less relevant since the single valley model is not realistic. At disorder radii near $\delta = 1$ nm, the maximum chain length Λ seems to saturate at a finite value. Analyzing the hopping distributions near this region and comparing it with those of exaggeratedly large radii ($\delta \approx 3$ nm), we see that in fact this is not a fully converged value for Λ. This plateau is accidental, and larger δ will lead to a higher probability of vanishingly small hoppings, thus obtaining the expected limit of $\Lambda(\delta \to \infty) = 0$.

Figure 5 presents the density of states (DOS) averaged over an ensemble of 10^4 samples of chains with $\approx$500 nm, differentiating single valley and multivalley models. For comparison the target chain DOS is also shown. No significant differences are observed comparing the two models of disorder (2D and 3D). On the other hand, effects coming from valley interference may be observed in the DOS, where we note that the single valley DOS for small δ shows close similarities to that of 1D ordered chains, while, as δ increases, the energy range of the spectrum widens and the peak related to the 1D Van Hove–like peak lowers and spreads. In the single valley model, disorder is responsible for washing the Van Hove singularity away slowly, keeping a remainder of the idealized chain peak at the band edge [27]. Only at disorder levels comparable to the donor separation does the Van Hove singularity fully disappear. Meanwhile, for the multivalley cases, the relevant length parameter leading to the extinction of the singularity fingerprint is the oscillation period $2\pi/k_0$. Therefore, even the smallest positioning disorder (a single atomic spacing) is enough to eliminate this feature. Contrary to models where the disorder is tuned by a continuous parameter [27], multivalley DOS has no remanent features of the ordered 1D character, no memory of Van Hove singularities at the

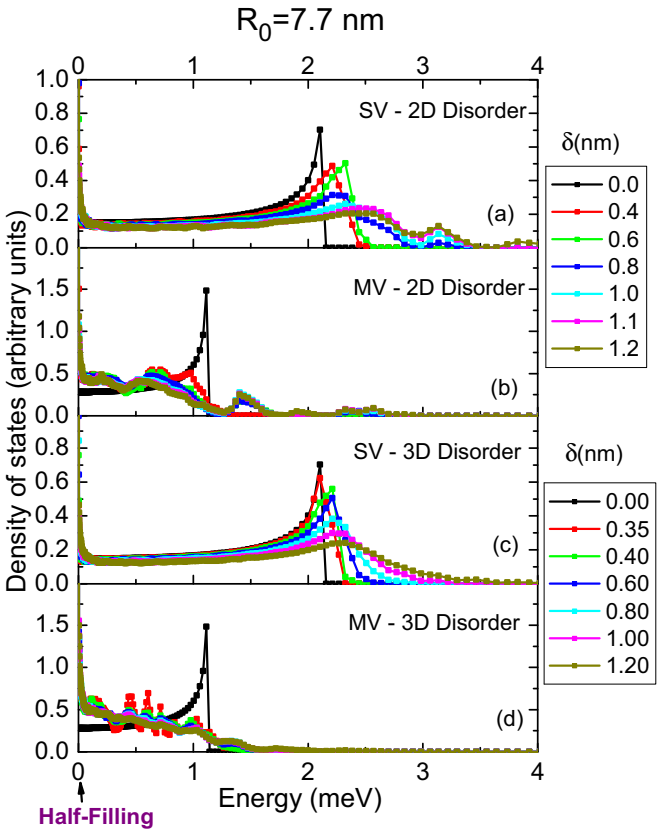

FIG. 5. Density of states in energy for six different disorder radii (δ). Our model leads to a single band which is symmetric around the on-site energy ϵ, taken to be zero here. The model (SV or MV, 2D or 3D) is indicated in each frame. The DOS for the target chain configuration is also given ($\delta = 0$).

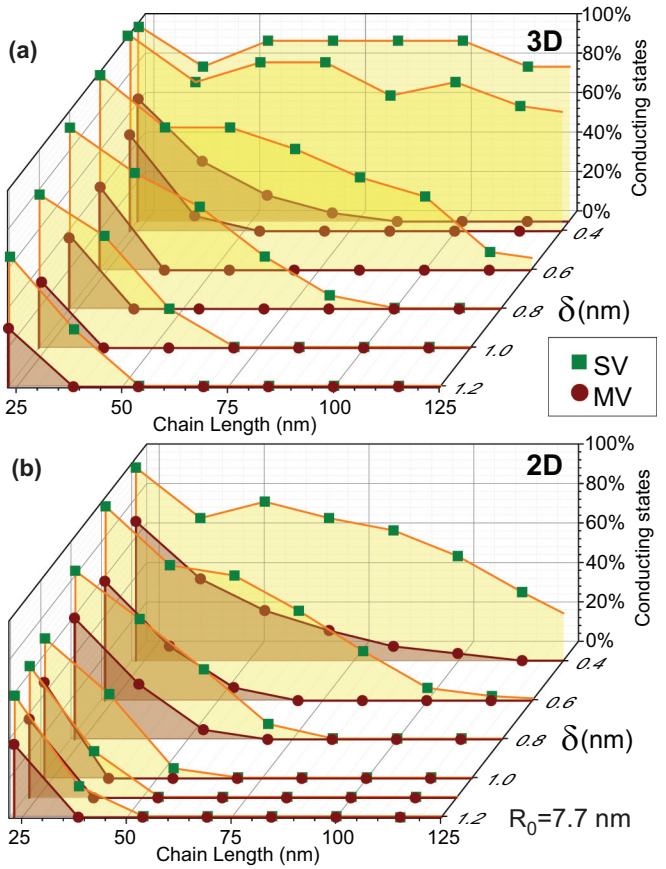

FIG. 6. Fraction of conducting states as a function of donor chain length (L and the disorder radius (δ) for the single valley (SV) and multivalley (MV) models. The 3D disorder model (a) and the 2D disorder model (b) were considered. Results are presented for a distance of 7.7 nm between target implantation points.

edges of the energy spectrum. It is possible to observe that the multivalley DOS presents sharp oscillations for small δ that become smoother as δ increases.

Note that the DOS in the multivalley cases increases towards the band center as compared to the respective single valley DOS, which increases toward the edges. In all cases the DOS has a peak at the center of the spectrum, i.e., the isolated-donor energy $\epsilon = 0$. It is long known that in the case of purely off diagonal disorder in one dimension the state at the center of the band is not exponentially localized [28]. While it still decays with distance, it is slower than the decay in Eq. (9). This favors the existence of longer localization lengths around the center of the spectrum.

While the mobility edge is reduced in multivalley materials due to valley interference, this accumulation of states near the band center favors transport. In our simulations we did not find any instances in which the latter effect is more relevant than the first. In other words, the number of conducting states is always larger in single valley materials.

A comprehensive summary of our results is given in Fig. 6. We analyze localization properties of chains with fixed target donors distance $\mathbf{R}_0$ along [110]. Ensembles are grouped by disorder δ and length L, where δ characterizes 2D or 3D position distributions and consequently tunnel coupling distributions. Single valley and multivalley models are also treated independently. Overall we studied about 200 ensembles, corresponding to a fixed combination [δ, L, dimension of disorder (2D or 3D), valley multiplicity (single or multi)]. The conduction character of each statistical realization is verified according to our criterion. The data points in the figure give the fraction of conducting samples in the respective ensemble.

VIII. FINAL REMARKS AND CONCLUSIONS

Our study reveals nontrivial and sometimes unexpected consequences of fabrication parameters ($\mathbf{R_0}$ and L) and fabrication control (δ) on the transport behavior of 1D donor chains in silicon. Trends and properties described here are likely to be found in experimental investigations. The main difficulty, to be overcome in the future, is to generate a large enough set of samples where the statistical search presented here could be performed.

Our results are consistent with relatively long conducting chains reported in experiments, [1] even in disordered cases driven by valley interference effects (Fig. 3). Distances between donors are reasonably controllable within STM-tip deposition techniques while the disorder radius is continually reduced with the development of these techniques [29–33].

In our model, the Coulomb electron-electron correlations are not explicitly included. However, in the context of low-dimensional systems like P-donor arrays in Si, explicit inclusion of electron-electron correlations are known to affect the electronic behavior and may eventually dominate the transport behavior [32]. Nonetheless, the trends found here are expected to contribute to highly correlated chains, for which a detailed inclusion of the geometrical disorder and multivalley effects may not be trivial.

ACKNOWLEDGMENTS

We are indebted to S. Queiroz for the many discussions on the TMA. The authors also thank R. Scalettar for lively discussions. This work is part of the Brazilian National Institute for Science and Technology on Quantum Information. The authors also acknowledge partial support from Fundação Carlos Chagas Filho de Amparo à Pesquisa do Estado do Rio de Janeiro (FAPERJ), Conselho Nacional de Desenvolvimento Cientifico e Tecnológico (CNPq), and Coordenação de Aperfeiçoamento de Pessoal de Nível Superior (CAPES).

APPENDIX: COMPUTING LYAPUNOV EXPONENTS AND INTEGRATED DENSITY OF STATES (IDOS): 1D CHAIN WITH OFF-DIAGONAL DISORDER

Considering the linear mapping presented in Eq. (10c), numerical implementation faces two main difficulties. In obtaining a final Lyapunov vector (LV) $\widehat{\Phi}_{L-1}$, one has to handle the product $\widehat{P}_L \cdot \widehat{\Phi}_0$ that diverges exponentially dominated by the Lyapunov maximum exponent (LME)—exceeding the overflow limit. The other difficulty is related to the fact that the $\widehat{\Phi}_{L-1}$ asymptotic direction is given by the Oseledec subspace related to the LME, i.e., for any initial vector $\widehat{\Phi}_0$, the angle between final Lyapunov vectors will tend to zero leading to determinant precision problems [34].

In this work, the solution for these difficulties lies in extracting the increase and decrease of LV associated with the LME and the LmE (Lyapunov minimal exponent), respectively. For this purpose we made use of the Gram-Schmidt orthonormalization procedure (GSOP)—in the usual diagonal disorder context this procedure is implemented after m steps but since in our problem the LVs diverge faster it will be done after each step. Although the procedure will be more expensive computationally it will impact in a very convenient way to determine the IDOS by the node counting technique.

We begin the GSOP initializing the LV, i.e., we randomly choose an initial set of orthonormal LVs: $(\widehat{\Phi}_0^{(1)}, \widehat{\Phi}_0^{(2)})$. After each step we extract the modulus of these LVs and this set is orthonormalized again, for a $k+1$ step,

$$\widehat{\Phi}_{k+1}^{(1)} = \frac{\widehat{T}_{k+1} \cdot \widehat{\Phi}_k^{(1)}}{M_{k+1}^{(1)}}, \tag{A1a}$$

$$\widehat{\Phi}_{k+1}^{(0)} = \frac{\left[\widehat{1} - \widehat{\Phi}_{k+1}^{(1)} \widehat{\Phi}_{k+1}^{(1)\dagger}\right] \widehat{T}_{k+1} \cdot \widehat{\Phi}_k^{(0)}}{M_{k+1}^{(0)}}, \tag{A1b}$$

where $(M_{k+1}^{(p=1,0)})$ is the modulus of each LV before the normalization procedure. The LME ($p=1$) and LmE ($p=0$) will be given by

$$\gamma^{(p)} = \frac{1}{L} \sum_{i=0}^{L-1} \frac{\ln\left[M_i^{(p)}\right]}{|\mathbf{R}_i|}, \tag{A2}$$

where L is the chain length and $\mathbf{R}_i$ is the vector connecting a pair of nearest-neighbor donors (i and $i+1$). Although we apply an orthonormalization procedure to the set of LVs it is good to clarify that this set is not necessarily orthogonal; the goal here is to decrease the influence of the LME in determining LVs associated with other Lyapunov exponents.

In our model, the nth eigenstate must have n nodes and given this, the number of states below the energy given by nth eigenstate will be precisely n. By the node counting technique we determine the IDOS by the ratio of the wave function amplitudes (ϕ_n) presented in Eq. (10a), i.e.,

$$\mathrm{IDOS}(E) = \frac{1}{L} \sum_{i=0}^{N-1} \Theta\left[-\frac{\phi_i(E)}{\phi_{i+1}(E)}\right]; \tag{A3}$$

Θ is the Heaviside theta. By the IDOS the density of states is easily obtained.

[1] B. Weber, S. Mahapatra, H. Ryu, S. Lee, A. Fuhrer, T. C. G. Reusch, D. Thompson, W. C. T. Lee, G. Klimeck, L. C. L. Hollenberg, and M. Y. Simmons, Science **335**, 64 (2012).
[2] B. Weber, H. Ryu, Y.-H. M. Tan, G. Klimeck, and M. Y. Simmons, Phys. Rev. Lett. **113**, 246802 (2014).
[3] T. Shinada, S. Okamoto, T. Kobayashi, and I. Ohdomari, Nature (London) **437**, 1128 (2005).
[4] E. Prati, M. Hori, F. Guagliardo, G. Ferrari, and T. Shinada, Nat. Nano **7**, 443 (2012).
[5] E. Prati, K. Kumagai, M. Hori, and T. Shinada, Sci. Rep. **6**, 19704 (2016).
[6] O. Madelung, *Semiconductors: Data Handbook* (Springer Science & Business Media, New York, 2012).
[7] J. M. Luttinger and W. Kohn, Phys. Rev. **97**, 869 (1955).
[8] C. Kittel and A. H. Mitchell, Phys. Rev. **96**, 1488 (1954).
[9] A. L. Saraiva, J. Salfi, J. Bocquel, B. Voisin, S. Rogge, R. B. Capaz, M. J. Calderón, and B. Koiller, Phys. Rev. B **93**, 045303 (2016).
[10] A. L. Saraiva, A. Baena, M. J. Caldern, and B. Koiller, J. Phys.: Condens. Matter **27**, 154208 (2015).
[11] J. Slater, *Quantum Theory of Molecules and Solids*, International Series in Pure and Applied Physics Vol. 1 (McGraw-Hill, New York, 1963).
[12] M. V. Klymenko and F. Remacle, J. Phys.: Condens. Matter **26**, 065302 (2014).
[13] A. MacKinnon and B. Kramer, Phys. Rev. Lett. **47**, 1546 (1981).
[14] J. L. Pichard and G. Sarma, J. Phys. C **14**, L127 (1981).
[15] J. L. Pichard and G. Sarma, J. Phys. C **14**, L617 (1981).

[16] A. MacKinnon and B. Kramer, Z. Phys. B **53**, 1 (1983).
[17] B. Kramer and A. MacKinnon, Rep. Prog. Phys. **56**, 1469 (1993).
[18] K. M. Itoh, M. Watanabe, Y. Ootuka, E. E. Haller, and T. Ohtsuki, J. Phys. Soc. Jpn. **73**, 173 (2004).
[19] S. N. Evangelou, J. Phys. C **19**, 4291 (1986).
[20] I. Y. Gol'dsheid and G. A. Margulis, Russ. Math. Surv. **44**, 11 (1989).
[21] V. I. Oseledets, Trans. Moscow Math. Soc. **19**, 197 (1968).
[22] D. Ruelle, Ann. Math. **115**, 243 (1982).
[23] U. Krengel and A. Brunel, *Ergodic Theorems* (Cambridge University Press, Cambridge, England, 1985).
[24] R. Carmona and J. Lacroix, *Spectral Theory of Random Schrödinger Operators* (Springer Science & Business Media, New York, 2012).
[25] P. W. Anderson, Phys. Rev. **109**, 1492 (1958).
[26] B. Bulka, B. Kramer, and A. MacKinnon, Z. Phys. B **60**, 13 (1985).
[27] B. Koiller, M. Robbins, M. Davidovich, and C. E. T. G. da Silva, Solid State Commun. **45**, 955 (1983).
[28] C. M. Soukoulis and E. N. Economou, Phys. Rev. B **24**, 5698 (1981).
[29] K. Eng, R. McFarland, and B. Kane, Proceedings of the 16th International Conference on Electronic Properties of Two-Dimensional Systems (EP2DS-16), Physica E (Amsterdam, Neth.) **34**, 701 (2006).
[30] B. Hu, T. M. Kott, R. N. McFarland, and B. E. Kane, Appl. Phys. Lett. **100**, 252107 (2012).
[31] E. H. Hwang and S. Das Sarma, Phys. Rev. B **87**, 075306 (2013).
[32] S. Shamim, S. Mahapatra, G. Scappucci, W. M. Klesse, M. Y. Simmons, and A. Ghosh, Phys. Rev. Lett. **112**, 236602 (2014).
[33] Y.-L. Hsueh, H. Büch, Y. Tan, Y. Wang, L. C. L. Hollenberg, G. Klimeck, M. Y. Simmons, and R. Rahman, Phys. Rev. Lett. **113**, 246406 (2014).
[34] A. Crisanti, G. Paladin, and A. Vulpiani, *Products of Random Matrices*, Springer Series in Solid-State Sciences Vol. 104 (Springer, Berlin, 1993).